Journal Name

ARTICLE

Continuous-flow crystallisation in 3D-printed compact devices

Obinna Okafor,[a] Karen Robertson,[a] Ruth Goodridge[a] and Victor Sans*[a,b]

Received 00th January 20xx,
Accepted 00th January 20xx

DOI: 10.1039/x0xx00000x

www.rsc.org/

A flexible and cost-effective methodology to develop compact flow devices with heat exchange ability is presented here. Additive manufacturing techniques allows the rapid design and manufacturing of modular jacketed flow devices, where heat exchange can be modelled and controlled to generate efficient devices for applications in continuous-flow cooling crystallisation. As a proof of concept, the crystallisation of paracetamol has been demonstrated. The manufactured devices are effective to crystallise form II paracetamol employing metacetamol as co-crystallising agent.

Introduction

Crystallisation is a key unit operation in pharmaceutical industry and other high added value industrial processes.[1] The synthesis of reproducible and highly controlled crystals is critical for polymorphism and processability.[2] Polymorphic forms can display markedly different physicochemical properties such as density, chemical stability, solubility, hardness, melting point, rate of dissolution, hygroscopicity and interaction with biological systems.[3] Polymorphism in drug development is an important area of study as it contributes to the variability in active pharmaceutical ingredients (APIs), posing a challenge to scientists. Statistically, 50% of APIs have multiple forms, while 85% exhibit (pseudo)polymorphism,[3] which opens challenges to the engineering of 'tailor made' properties of an API. General selection criteria during an API development process aim for polymorphs with thermodynamic stability, good solubility and dissolution rate, non-hygroscopic and block-like habits for ease of manufacturing.[3, 4] Current knowledge on nucleation and crystal growth mechanisms and process are still insufficient to ensure precise control of formation and polymorph disappearance or phase transformation.[5]

Paracetamol (PC) is a widely used analgesic and antipyretic, which is commonly used to relieve aches and pains. It makes up part of cold and flu remedies and has been extensively studied in its solid state.[6] PC crystallises in three different polymorphs: Stable form I (monoclinic), metastable form II (orthorhombic) and unstable form III. Two other polymorphic forms are only accessed at high pressure. The layered structure of form II and the notably well-defined slip planes facilitate compressibility facilitating tableting and packaging, and increased solubility which improves bioavailability.[7, 8] There have been extensive studies in the production of both forms of paracetamol in both batch [8, 9] and continuous crystallisers: COBC,[10] MSMPR[11-13] and tubular.[14] Studied routes for the selective crystallisation of form II paracetamol include swift cooling,[15] reaction coupling,[13] enforcing Ostwald's rule of stages,[16] heterogenous nucleation,[17] use of polymer additives,[18, 19] separation in gel matrix [20] and multicomponent templating[7, 21]. Wilson *et al*. [21] demonstrated a new multi-component crystallisation route to selectively produce polymorphic form II by using auxiliary molecules, including benzoic acid derivatives and metacetamol (MCM), to perturb the solution environment encouraging its formation. Although the effect and mechanism of templating agents on the crystallisation process is not completely understood, it is proposed that the MCM affects the solution mediated phase transformation (form II to form I) that occurs during cooling.[7] It is also noted that the presence of the templating agent, MCM, has the effect of widening the metastable zone width of PC crystallisation.

Traditionally, batch crystallisation is the most common methodology employed. However, this presents important limitations related to batch to batch variability and mixing inefficiencies are important limitations. The development of continuous processes would be highly advantageous, despite the challenges of handling solids under flow.[22, 23] Continuous crystallisation offers rapid heat transfer and mass transfer benefits, as well as eliminating down time between batches.[10, 24] Continuous crystallisation processes can improve control of product properties and save production costs by up to 40 %. [25] There are important studies of continuous-crystallisers at the macroscale.[26, 27] The requirements for intensified mesoscale devices able to combine scalability and flexibility are very important for the development of industry 4.0 applications. Mesoscale devices might suffer from poor mixing as the dimensions are too large to ensure efficient mixing by diffusion and the crystalliser volumes are too low to enable residence times required for crystallisation at the high flow rates required to generate turbulent flow. Hence, the utilisation of advanced

[a] Faculty of Engineering, University of Nottingham, University Park, NG7 2RD, Nottingham, UK
[b] Institute of Advanced Materials (INAM), University Jaume I, 12041, Spain
Corresponding author: sans@uji.es
Electronic Supplementary Information (ESI) available: experimental details about methods and characterisation are included. See DOI: 10.1039/x0xx00000x

strategies to induce turbulent mixing at low flow rates represents a key requirement to develop efficient processing. However, the employment of traditional manufacturing techniques to generate necessary advanced features such as baffles is complicated.

Additive manufacturing (AM) represents an emerging set of technologies, which create objects, normally in a layer-by-layer fashion, directly from a 3D model file.[28] The application of AM to manufacture continuous-flow devices has attracted a great deal of interest in recent years.[29, 30] Recently, we demonstrated that AM can be employed to generate advanced meso-scale continuous-oscillatory baffled reactors for the controlled synthesis of nanoparticles.[31] We hypothesised that AM can be employed to generate advanced flow crystallisers. AM has two main potential benefits in mesoscale crystallisation process: i. enhanced mass transport with complex mixing architectures; ii. controlled heat transfer properties by designing the geometry of the crystalliser, wall thickness between crystallising solution and heat transfer media and the materials of construction. For instance, polymer materials have intrinsically low heat transfer coefficients, a graduated or controlled wall thickness can lead to gentle temperature profiles which can be crucial for targeting particular crystallisation pathways. Here, we present the first example utilising additive manufacturing to develop advanced devices with applications in continuous-flow crystallisers. The crystallisation of paracetamol is demonstrated as a benchmark.

A. AM fabrication of a flow reactor

Two flow crystallisers were designed for this work. The first was designed to characterise and model the heat transfer in the flow devices (Figure 1). The second was employed for the crystallisation of paracetamol. The devices were designed with Creo Parametric® CAD software and converted to STL (standard tessellation language), a common file format utilised on AM programmes. The geometry was then sliced into defined layers for manufacturing on PreForm software. The crystallisers were manufactured on a Vat polymerisation-based AM platform (Form 2 by Formlabs), using off-the-shelf Clear resin (RS-F2-GPCL-04). The Vat polymerisation platform was utilised for its suitability in manufacturing 3-dimensionally complex and intricate features at high resolution. The platform utilised allows features to be produced as fine as 25µm. The AM technique is beneficial in flow reactor fabrication as unreacted polymerisation mixtures are easily flushed out from the channels with isopropanol (IPA) immediately after manufacture. Two additively manufactured crystallisers (AMC), were manufactured with similar features, the difference being the diameter of the channels and the number of temperature sensing ports (

Table 1). The smaller diameter (AMC-I) device was used for heat transfer studies while the slightly larger (see Table 1 for comparison) was used for the crystallisation experimentation to avoid blockades and to increase residence time. The larger crystalliser, (AMC-II), was also designed to allow several reactors to be connected in series creating opportunities for longer residence time or multi-stage reactions. The crystallisers were manufactured with a large heat transfer chamber around the flow tubes in order to achieve close to isothermal conditions.

Using AM allowed a cost-effective method to fabricating bespoke crystallisers. For example, AMC-I crystalliser, which was manufactured with a layer resolution of 50 µm, using 209 mL of resin and fabrication time of 17.5h works out to £30 material cost. The device specifications are presented in

Table 1.

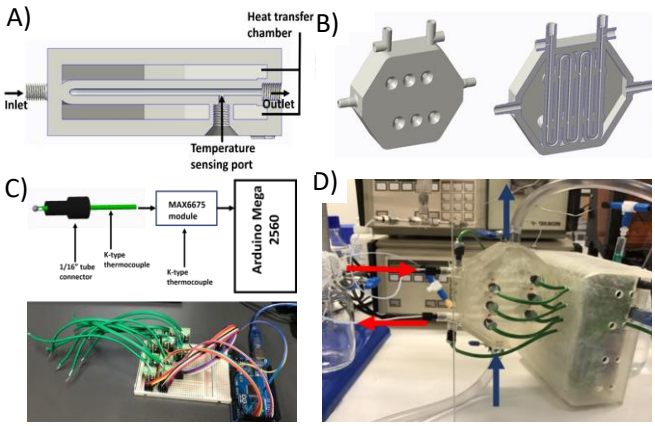

Figure 1 Schematic representation of additively manufactured crystalliser (AMC) designed and used for this work for the heat exchange modelling. A) Cross-section of the device, showing the heat-exchange chamber, the crystalliser channel and the temperature sensing ports. B) CAD model of the AMC-I crystalliser and a cross-section. C) Schematic design of the temperature measuring devices and a picture of the actual set-up. D) Rig set-up for heat transfer characterisation in the additively manufactured crystalliser. The set-up comprises a recirculating chiller, HPLC pump and temperature sensors connected to the crystallisers.

Table 1: Reactor design parameters

Parameter	Units	AMC-I	AMC-II
Reactor Volume	mL	2.08	2.95
Inner diameter D_i	mm	2.1	2.5
Outer diameter D_o	mm	9.0	9.0
Wall thickness	mm	3.45	3.25
Cooling jacket *V*	mL	158	170
Reactor dimensions	mm	155x118x32	165x118x32
Thermocouple ports	ZEA	14	4

B. Heat transfer studies and reactor modelling

A rig comprising a Gilson 307 HPLC pump connected *via* unheated 1/16" PTPE tubing and tube connectors to the crystalliser and a Julabo F250 recirculating chiller connected in a counter-flow direction to the device was set up to characterise the rate of heat transfer in the crystalliser (Figure 2A). Following

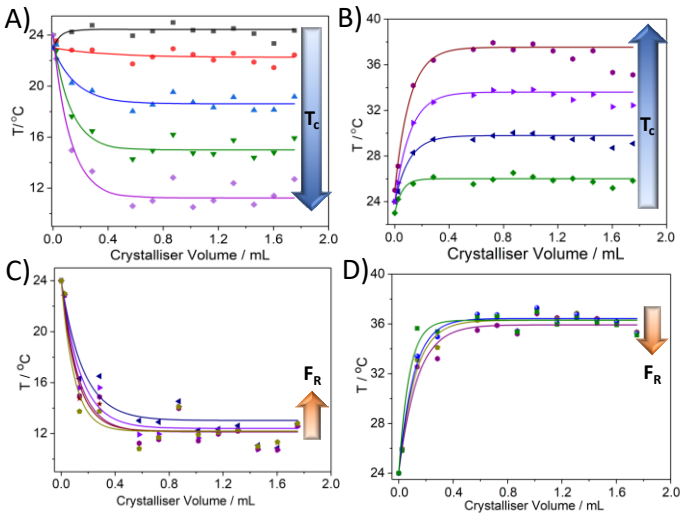

Figure 2 A-B) Temperature profile in the AMC at different recirculating temperatures at constant flow rate (0.5 ml min^{-1}). In all cases, the points correspond to experimental results and the lines correspond to the fitting to an exponential function. Chiller temperature (Tc) was increased in intervals of 5 °C, for B) Tc=5 °C (violet) to 23 °C (black) and C) from 25 °C (green) to 40 °C (burgundy). C-D) Temperature profile in the additively manufactured crystalliser at different flow rates at T_c=5°C (C) and T_c=40°C (D), where data points represent experimental measurements and the solid lines the fitting of the results to an exponential function. In C) the flow rates studied were 0.25 ml min^{-1} (yellow pentagons), 0.5 ml min^{-1} (burgundy hexagons), 1 ml min^{-1} (burgundy stars), 1.5 ml min^{-1} (violet right triangles) and 2 ml min^{-1} (blue left triangles). In D) the flow rates studied were 0.25 ml min^{-1} (green squares), 0.5 ml min^{-1} (blue spheres), 1 ml min^{-1} (yellow pentagons) and 2 ml min^{-1} (violet hexagons).

the trend of low cost control and automation chemical systems,[32] an off the shelf Arduino mega micro-controller was coupled with MAX6675 thermocouple sensor modules linked to thermocouple connectors (Figure 2E). The K-type thermocouples (*ca.* 2mm diameter) were attached to 1/16" tube connectors with control software coded with Labview to handle the data acquisition. The constant noise in the signal was smoothed employing a 5 point fast Fourier transform (FFT) algorithm, an example signal is presented Figure S2. The 14 thermocouples were placed at regular intervals (46 mm, equivalent to 0.16 mL) spanning from the inlet to the outlet of tubular channels (Figure 2D). The thermocouple connectors were designed to be in constant contact with the fluid flowing into the crystalliser at room temperature whilst monitoring the heat transfer as an effect of the jacketed fluid. Experiments were designed to monitor the behaviour of the crystalliser at varying flow rates and T_c in the range 5 °C to 40 °C, with the process fluid at room temperature. The concrete conditions explored are presented in section 2 and Table 1 in the SI. The second set of experiments were run at varying flow rates of 0.25 to 2 ml min^{-1} at 5°C and 40°C. The temperature of the chiller (T_C) was found to have a more significant effect (Figure 2B-C) in both cooling and heating experiments than the flow rates (Figure 2F-G). Generally, the data fitted well to exponential functions, which can be employed to model the system. Some thermocouples (e.g. at 0.9 mL) were showing a constant deviation to the rest of the trend, presumably due to a lack of intimate contact with the fluid. At the highest T_c explored, the trend was shown to deviate to lower temperatures towards the end of the channel. This is probably due to poor insulation or heat transfer. However, this does not affect the results, since cooling crystallisation was employed in the subsequent experiments. A reduction in the steepness of the curves was observed when the flow rate was increased both in cooling (Figure 2F) and heating (Figure 2G) experiments. With an increase in flow rate, there is reduced time for convective heat transfer to occur between the fluid and the crystalliser wall. The overall heat transfer in this case relates to the sum of the heat transfer by conduction and advection. Changing the flow rate provides a method of controlling the steep drop in temperature in the crystalliser. A slow temperature drop will be beneficial in controlling crystal formation and growth. The simplified models and computation methods are based on a set of assumptions summarised in equations E1-3. Modelling of the collected data was carried out using the following heat transfer equation:

$$\frac{T_s - T_{m,o}}{T_s - T_{m,i}} = exp\left[-\frac{PLU}{\mu c_p}\right] \quad \text{E1}$$

$$U = \left(\frac{1}{h_i} + \frac{1}{h_o}\right)^{-1} \quad \text{E2}$$

$$h = \frac{Nu.k}{D_h} \quad \text{E3}$$

$$Nu = 0.023.Re^{0.8}\left(\frac{\mu c_p}{k}\right)^{0.3} \quad \text{E4}$$

$$T_{m,o} = A.T_\infty - \left[A.T_\infty - T_{m,i}\right].exp\left[-\frac{PLU}{\mu cp}\right] \quad \text{E5}$$

$$Q = \frac{2\pi k}{\ln(r_2/r_1)}.(T_1 - T_2) = \frac{2\pi k}{\ln(r/r_1)}.(T_1 - T) \quad \text{E6}$$

Where T_s is the temperature at the tube internal surface, $T_{m,i}$ and $T_{m,o}$ represents the temperature at the middle inlet and outlet of the tube. P is the perimeter, L is the tube length, m is the mass flow rate, μ is the dynamic viscosity, k is the thermal conductivity, Re is the Reynold number, D_h is the hydraulic diameter, A is the correction factor U is the overall heat transfer coefficient, c_p is the heat capacity of the fluid, h_i and h_o are the convective heat transfer coefficient of the internal and external fluid. Nu corresponds to the Nusselt number. Nu value of 3.66 was used for the h_i calculation, an approximation for fully developed laminar flow, while equation 4 was used for Nu_o calculation.

For modelling purposes, the equation was simplified by assuming a linear relation between the outside temperature in the heat transfer chamber, T, and the internal surface temperature.

Thermal conductivity (k) measurements were carried out on 3-5 mm blocks of the AM resin material employed. This was done on a TCi Thermal Conductivity Analyzer utilising a Modified transient plane source (MTPS) sensor. The thermal conductivity (k) value obtained was 0.45±0.09 W m^{-1} K^{-1}. All measurements were conducted under steady state.

Even with the inherent experimental error introduced by the sensors and the limitations due to insufficient heat insulation at some points of the AMC, the modelled temperature of the internal surface, T_S, correlates linearly to the chiller

temperature, T_C (Figure 3A). The slope indicates a difference between the two values due to the heat loss in the tubing between the chiller and the AMC.

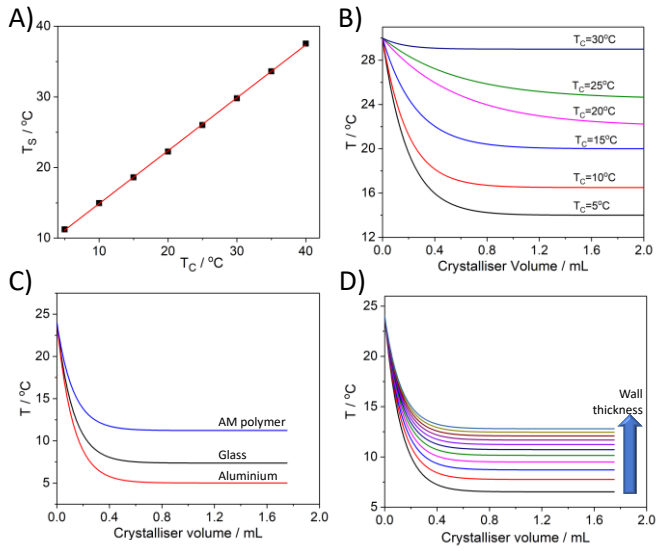

Figure 3. Modelling of AMC. A) Correlation between the temperature on the surface of the channels (T_S) and the temperature of the chiller (T_C). B) Simulation of cooling profiles for a crystallisation process in the AMC with an inlet temperature T_0 = 30 °C, 0.5 mL min^{-1} and different values of T_C indicated in the graph. C-D) Cooling profiles at T_C= 5 °C and 0.5 mL min^{-1} for materials with different heat conductivity (C) and with wall thicknesses ranging from 0.45 mm to 5.45 mm (0.5 mm increment) (D).

The modelling of the system allows comparison of the effect of different parameters without the need for experimentation, including the wall thickness, and to compare the cooling profiles of the acrylate-based material employed to manufacture the AMC to typical materials employed to manufacture crystallisers, like glass or aluminium (Figure 3C). Profiles of the modelled temperature change in the AMC at T_C=5 °C (cooling) for a wall/tube thickness ranging from 0.45mm to 5.45 mm were calculated (Figure 3D). Increasing the thickness of the wall increases the resistance to heat transfer by conduction. Hence, a less steep temperature drop was shown with the increase in wall thickness and *vice versa*. Similar results can be seen in both cooling and heating curves (Figure S3). As there are differences in thermal conductivity between the cured resin and glass or aluminium, there is a much reduced gradient of temperature before it plateaus. The less steep gradient is perceived to provide suitable conditions for selective crystallisation of single Paracetamol polymorphs. Figure 3B models the cooling profiles that can be observed in the experimental crystallisation of paracetamol discussed in section C.

C. Crystallisation experimentation and studies

A multi-component cooling crystallisation route to obtain paracetamol was explored in the AMC. This was achieved through recrystallisation of an aqueous Isopropyl alcohol solution (IPA) of purchased Paracetamol form I, with a high concentration of Metacetamol (MCM) to assist the crystallisation (see Figure S6 & S7 for a diffractogram).[10] All chemicals were purchased from Sigma Aldrich. MCM served as an additive which was to be retained in the effluent as MCM-hydrate. PC concentration of 300mg g^{-1} of solvent, combined with 25 wt % of MCM was dissolved in a mixture of 60:40 H_2O/IPA (v/v). The solution was stirred at 70 °C for 60 mins to equilibrate before beginning the cooling re-crystallisation process.[10]

The set-up consists of a hot plate, a Tricontinent C3000 syringe pump, a Julabo F250 recirculating chiller, the AMC-II equipped with four K-type thermocouples connected to an Arduino Mega for thermal control and a Buchner funnel flask connected to an low vacuum pump for filtration of the effluent (Figure 5). To control the temperature, preventing unwanted crystallisation prior to the AMC-II crystalliser and to allow for ease of cleaning, the 5 mL syringe of the Tricontinent pump was jacketed with a heating mat controlled with a PID controller coupled with a thermocouple. The control and monitoring of the system was carried out on with Labview. The experiment sequence involved pumping the heated aqueous IPA at 70 °C, with the syringe pump jacket at 60 °C through the fabricated crystalliser and then switching to the PC solution when conditions reached steady state. Recrystallisation experiments were run at cooling T_c ranging from 30 °C to 0 °C for 20 min in the first run and 60 min in the second run, (See Table S2). The experiments were run at a flow rate of 0.5 ml/min resulting in a residence time of 5.9 min. The filtered materials were collected at 20 min intervals, see Table S2 for more experimental details. The temperature at the inlet was observed to be 30 °C throughout all experimentation, allowing for nucleation and crystal growth at defined cooling rates to occur in the crystalliser. The predicted temperature profile in the reactor is presented in Figure 3B. It is important to highlight that, as a syringe pump was used in this experiment, there was an observed dip in the temperature during refill mode (see Figure S6). The time required to refill the pump was kept to a minimum with a high extraction rate (15 ml min^{-1}), which refilled the 5 ml syringe in 20 seconds. Further increase in the extraction rate resulted in cavitation. This is a limitation of the current experimental set-up, since the liquid becomes stagnant during the short time the syringe is being refilled.

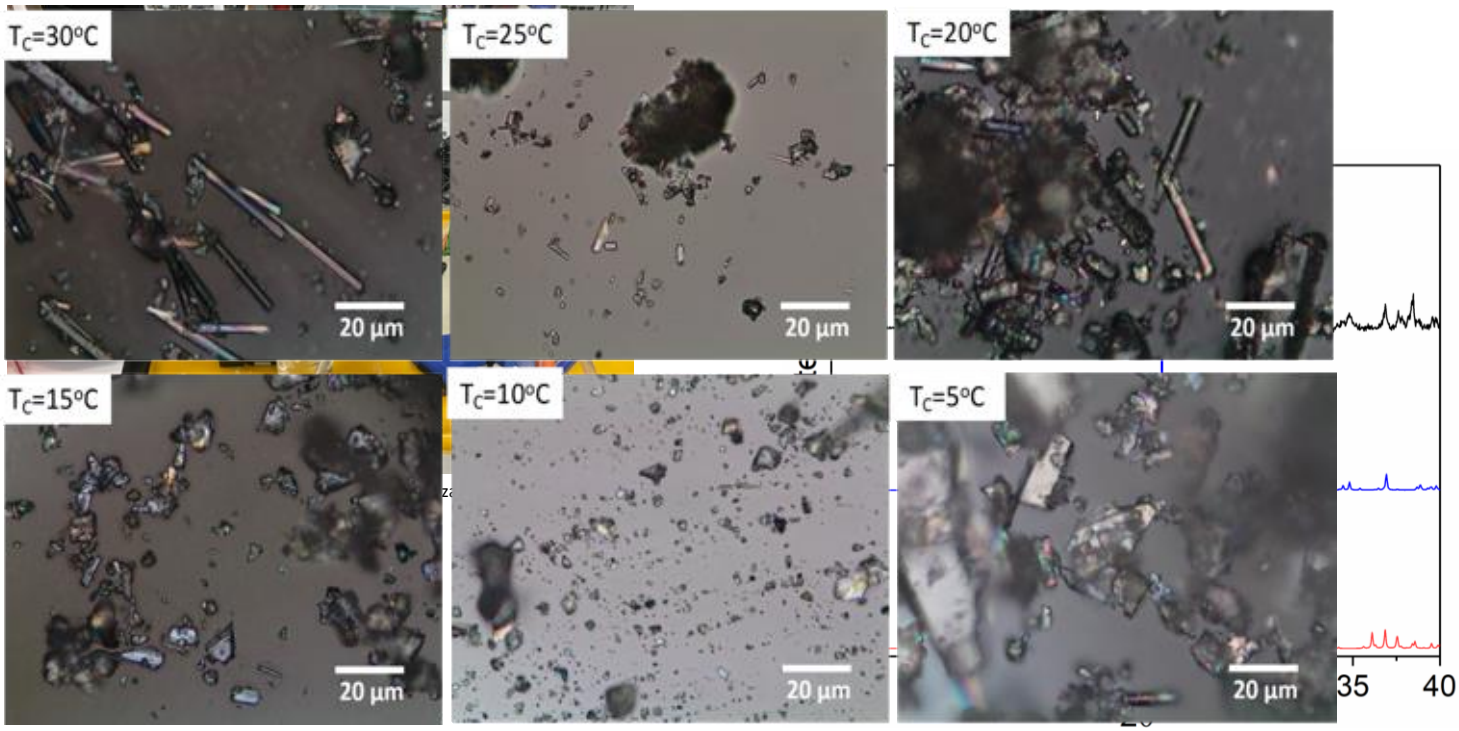

Figure 6 Optical images of collected samples at various cooling rates. Crystals can be observed in the images and the shape changes can be observed at varying chiller temperatures (T_C). Images are at 5X magnification.

The materials were characterised by optical microscopy and PXRD to establish the crystalline form of the recovered material. High resolution images were collected with Olympus BX51 optical microscope coupled with a 5X and 10X magnification lenses with a polariser filter attached to demonstrate the formation of crystals. No in-line process analytical techniques (PAT)[14, 33] were employed due to the clogging of the UV-Vis flow cell. The images collected with optical microscopy (Figure) show a clear indication of crystal formation. Both isolated crystals and clusters can be observed from the images. The images collected from the higher temperature runs (20-30 °C) seem to show the formation of more needle-like crystals, while a rhombic shape can be seen in the samples obtained from lower temperatures (5 °C to 15 °C). A transition of the crystal shape can be seen across the tested temperature range.

Powder X-ray diffraction (PXRD) patterns were collected using a Panalytical MPD X-ray diffractometer with primary monochromatic radiation (Cu-Kα1, λ = 1.5406A). The X-ray generator was run at 40 kV and 40 mA. The samples were mounted on brass plates and exposed over the range of 5° to 70° 2θ for 10.5 minutes per sample (continuous scan rate of 0.103 per sec). The collected samples were compiled and compared to reported reference patterns: CSD reference HXACAN01 – PC monoclinic form I, HXACAN26 - PC orthorhombic form II and MENSEE – MCM form I.

A close match can be observed between the reference starting material and the pure PC (I) purchased as well as the pure MCM and reference (Figure S7 and S8). The collected samples in contrast showed a large proportion of PC form II, as evidenced by the diffraction patterns of the collected samples (see Figure 7 for a representative example and the SI for the rest of diffractograms, section S5).

The peaks and comparison to collected samples are presented in Table S3 and in the SI. For all the samples analysed in both set of experiments, there are significantly larger amount of form II than form I identified. A reduction in the expression of PC form II peaks was observed in the second set of experiments at 10 min into the run at a T_c of 0 °C and 5 °C. Samples collected at 30 min and 60 min matched closely suggesting that the process may require some time to achieve steady state. Peaks of MCM can be observed to increase with an increase in process time at T_c 10 °C and 0 °C, regardless of the replacement of the Buchner funnel and filter paper every 20 mins to avoid blocking. The collected data does not allow a straightforward quantification and unfortunately well-defined melting points were not observed through DSC.

Figure 7. Representative XRD diffractogram T_C = 5 °C (black line), compared to simulated spectra for form I (red line) and form II (blue line).

These results are quite remarkable, since there are limited examples in the literature where polymorphs where controlled under continuous-flow by pre-selecting an adequate nucleation temperature.[34]

Problems related to fouling and seeding, common to continuous-flow crystallisers, were observed. High amounts of MCM were observed in the collected samples, indicating the occurrence of seeding, fouling or back-mixing in the crystalliser. The same crystalliser was used for the second set of experiments at 10 °C, 0 °C and 5 °C in that order for 60 minutes each. The experiments carried out at 5 °C quickly blocked the AMC in 30 min. Although the crystalliser was cleaned before each run, the blockage may have been as a result of build-up of fouling. This correlates with the high concentration of MCM observed at this final run. High counts of MCM and matching peaks can be observed in the compiled diffractograms in the SI section 5. In previous work we observed fouling during the synthesis of Ag nanoparticles in the AM fabricated continuous flow reactor with similar geometry to the AMC.[31] The non-smooth finishing of the printed surfaces would generate a higher surface area with points of reduced free energy for secondary nucleation and therefore crystallisation on the walls of the flow device. Furthermore, the pulsation of the pump generates non-steady state conditions in which the liquid becomes stagnant, thus facilitating the precipitation of solids on the crystalliser. These limitations might be overcome with advanced mixing reactor architectures, like meso-oscillatory baffled reactors (mOBRs) and pulsation-free reactors which have been applied for the synthesis of crystalline pure nano and microstructured materials.[35-37]

Conclusions

The fabrication of a mesoscale crystalliser for Paracetamol crystallisation utilising Additive Manufacturing (AM) has been demonstrated. Stereolithography based AM aided the fabrication of bespoke mesoscale flow devices near net shape geometry at studied parameters. The AMC designed with temperature sensing ports was manufactured and utilised in the study to selectively obtain a desirable polymeric form of Paracetamol. The heat transfer was modelled to achieve an in-depth understanding of the cooling dynamics in the AMC geometries.

Crystallisation of PC was selected as a benchmark study. The formation of PC in the crystalliser was studied under varying temperatures. The cooling crystallisation process carried out in the crystalliser allowed the production of PC crystals under continuous-flow. This represents the first example of continuous PC crystallisation carried out in an AM crystalliser at such scale. The preliminary results obtained suggest a control over the polymorphism in the cooling crystallisation of paracetamol. In this case, the kinetically controlled form II was the major crystalline form observed despite previous reports of this polymorphic form requiring very specific crystallisation conditions. This work will open the door to new and creative ways to design and manufacture advanced crystallisers to work as stand-alone unit operations or coupled to flow chemical reactors.

Acknowledgements

The Generalitat Valenciana, project CIDEGENT/2018/036 is gratefully acknowledged. The authors want to acknowledge the EPSRC EP/I033335/2 grant for funding.

Notes and references

1. B. Y. Shekunov and P. York, *Journal of Crystal Growth*, 2000, **211**, 122-136.
2. M. Leane, K. Pitt and G. Reynolds, *Pharmaceutical Development and Technology*, 2015, **20**, 12-21.
3. P. H. Karpinski, *Chemical engineering & technology*, 2006, **29**, 233-237.
4. C. Sudha and K. Srinivasan, *Journal of Crystal Growth*, 2014, **401**, 248-251.
5. D.-K. Bučar, R. W. Lancaster and J. Bernstein, *Angewandte Chemie International Edition*, 2015, **54**, 6972-6993.
6. G. G. Zhang, D. Law, E. A. Schmitt and Y. Qiu, *Advanced drug delivery reviews*, 2004, **56**, 371-390.
7. L. R. Agnew, D. L. Cruickshank, T. McGlone and C. C. Wilson, *Chemical Communications*, 2016, **52**, 7368-7371.
8. I.-C. Wang, M.-J. Lee, D.-Y. Seo, H.-E. Lee, Y. Choi, W.-S. Kim, C.-S. Kim, M.-Y. Jeong and G. J. Choi, *Aaps Pharmscitech*, 2011, **12**, 764-770.
9. M. Fujiwara, P. S. Chow, D. L. Ma and R. D. Braatz, *Crystal Growth & Design*, 2002, **2**, 363-370.
10. L. R. Agnew, T. McGlone, H. P. Wheatcroft, A. Robertson, A. R. Parsons and C. C. Wilson, *Crystal Growth & Design*, 2017, **17**, 2418-2427.
11. K. A. Powell, A. N. Saleemi, C. D. Rielly and Z. K. Nagy, *Chemical Engineering and Processing: Process Intensification*, 2015, **97**, 195-212.
12. G. Hou, G. Power, M. Barrett, B. Glennon, G. Morris and Y. Zhao, *Crystal Growth & Design*, 2014, **14**, 1782-1793.
13. G. Power, G. Hou, V. K. Kamaraju, G. Morris, Y. Zhao and B. Glennon, *Chemical Engineering Science*, 2015, **133**, 125-139.
14. V. Sans and L. Cronin, *Chemical Society Reviews*, 2016, **45**, 2032-2043.
15. C. Sudha and K. Srinivasan, *CrystEngComm*, 2013, **15**, 1914-1921.
16. J. C. Burley, M. J. Duer, R. S. Stein and R. M. Vrcelj, *European Journal of Pharmaceutical Sciences*, 2007, **31**, 271-276.
17. K. Chadwick, A. Myerson and B. Trout, *CrystEngComm*, 2011, **13**, 6625-6627.
18. W. Kaialy, H. Larhrib, B. Chikwanha, S. Shojaee and A. Nokhodchi, *International Journal of Pharmaceutics*, 2014, **464**, 53-64.
19. C. Sudha, R. Nandhini and K. Srinivasan, *Crystal Growth & Design*, 2014, **14**, 705-715.
20. C. Sudha, P. Parimaladevi and K. Srinivasan, *Materials Science and Engineering: C*, 2015, **47**, 150-155.
21. L. H. Thomas, C. Wales, L. Zhao and C. C. Wilson, *Crystal Growth & Design*, 2011, **11**, 1450-1452.
22. R. L. Hartman, *Organic Process Research & Development*, 2012, **16**, 870-887.

23. V. Sebastian, S. A. Khan and A. A. Kulkarni, *Journal of Flow Chemistry*, 2017, **7**, 96-105.
24. S. Lawton, G. Steele, P. Shering, L. Zhao, I. Laird and X.-W. Ni, *Organic Process Research & Development*, 2009, **13**, 1357-1363.
25. S. D. Schaber, D. I. Gerogiorgis, R. Ramachandran, J. M. B. Evans, P. I. Barton and B. L. Trout, *Industrial and Engineering Chemistry Research*, 2011, **50**, 10083-10092.
26. T. McGlone, N. E. B. Briggs, C. A. Clark, C. J. Brown, J. Sefcik and A. J. Florence, *Organic Process Research & Development*, 2015, **19**, 1186-1202.
27. A. J. Alvarez and A. S. Myerson, *Crystal Growth & Design*, 2010, **10**, 2219-2228.
28. A. J. Capel, S. Edmondson, S. D. Christie, R. D. Goodridge, R. J. Bibb and M. Thurstans, *Lab on a Chip*, 2013, **13**, 4583-4590.
29. V. Sans, V. Dragone and L. Cronin, in *Handbook of Green Chemistry*, ed. P. T. Anastas, 2019, DOI: 10.1002/9783527628698.hgc141.
30. P. J. Kitson, M. H. Rosnes, V. Sans, V. Dragone and L. Cronin, *Lab on a Chip*, 2012, **12**, 3267-3271.
31. O. Okafor, A. Weilhard, J. A. Fernandes, E. Karjalainen, R. Goodridge and V. Sans, *Reaction Chemistry & Engineering*, 2017, **2**, 129-136.
32. F. Zhao, D. Cambié, V. Hessel, M. G. Debije and T. Noël, *Green Chemistry*, 2018, **20**, 2459-2464.
33. G. A. Price, D. Mallik and M. G. Organ, *Journal of Flow Chemistry*, 2017, **7**, 82-86.
34. B. Rimez, R. Debuysschère, J. Conté, E. Lecomte-Norrant, C. Gourdon, P. Cognet and B. Scheid, *Crystal Growth & Design*, 2018, **18**, 6431-6439.
35. V. Sans, S. Glatzel, F. J. Douglas, D. A. Maclaren, A. Lapkin and L. Cronin, *Chemical Science*, 2014, **5**, 1153-1157.
36. C. J. Richmond, H. N. Miras, A. R. de la Oliva, H. Zang, V. Sans, L. Paramonov, C. Makatsoris, R. Inglis, E. K. Brechin, D.-L. Long and L. Cronin, *Nature Chemistry*, 2012, **4**, 1037.
37. K. Kastner, A. J. Kibler, E. Karjalainen, J. A. Fernandes, V. Sans and G. N. Newton, *Journal of Materials Chemistry A*, 2017, **5**, 11577-11581.